SCS
Swiss Chemical
Society

HELVETICA
chimica acta

Accepted Article

Title: Intramolecular Charge-Transfer Dynamics in Benzodifuran-Based Triads

Authors: Stephan Keller, Jihane Hankache, Oleksandr Yushchenko, Latévi Max Lawson Daku, Qinchao Sun, Jie Ding, Silvio Decurtins, Eric Vauthey, Robert Häner, Andreas Hauser, and Shi-Xia Liu

To be cited as: *Helv. Chim. Acta* 10.1002/hlca.202100099

Link to VoR: https://doi.org/10.1002/hlca.202100099

www.helv.wiley.com

WILEY-VHCA

Helvetica Chimica Acta
HELVETICA
10.1002/hlca.202100099

Intramolecular Charge-Transfer Dynamics in Benzodifuran-Based Triads

Stephan Keller,[a] Jihane Hankache,[b] Oleksandr Yushchenko,[b] Latévi Max Lawson Daku,[b] Qinchao Sun,[b] Jie Ding,[b] Silvio Decurtins,[a] Eric Vauthey,[b] Robert Häner,[a] Andreas Hauser,*[,b] and Shi-Xia Liu*[,a]

[a] Department of Chemistry, Biochemistry and Pharmaceutical Sciences, University of Bern, Freiestrasse 3, CH-3012, Bern, Switzerland, e-mail shi-xia.liu@unibe.ch

[b] Department of Physical Chemistry, University of Geneva, 30 Quai Ernest Ansermet, CH-1211 Geneva, Switzerland, e-mail Andreas.Hauser@unige.ch

This work is dedicated to Peter Kündig on the occasion of his 75th birthday

A facile and efficient approach for the synthesis of new conjugated donor-π-acceptor (D-π-A) chromophores has been developed, in which benzodifuran (BDF) and/or triphenyl amine (TPA) units are the donor moieties, linked by ethylenic bridges to electron-deficient anthraquinone (AQ) and 11,11,12,12-tetracyano-9,10-anthraquinodimethane (TCAQ) as the acceptor moieties. The resultant triads either with a symmetric A-D-A or an asymmetric D'-D-A structure show intense absorption bands in the visible spectral region due to efficient intramolecular charge transfer (ICT) from the HOMO localized on the BDF core to the LUMO localized on the AQ or the TCAQ unit. Electronic interactions between these redox-active components were studied by a combination of cyclic voltammetry, spectroelectrochemistry, UV-visible and ultrafast transient absorption spectroscopy. Analysis of the femtosecond excited-state dynamics reveal that all triads undergo a rapid charge recombination process which occurs within a few picoseconds, indicating that ethylenic linkers can facilitate electron delocalization among BDF and AQ/TCAQ units and thus impart effective electronic interactions between them.

Keywords: benzodifuran • donor-acceptor ensemble • intramolecular charge-transfer • spectroelectrochemistry • ultrafast optical spectroscopy

Introduction

Benzodifuran (BDF) derivatives have been explored intensively to serve as semiconductors in organic field effect transistors (OFETs) and chromophores in organic light-emitting diodes (OLEDs) and photovoltaics due to their fascinating structural features and intrinsic electronic properties.[1-11] Particularly, the planar and cruciform geometry of BDF provides a simple and versatile strategy for facilitating electron delocalization along a long (2,6-positions) or short (4,8-positions) axis and for gradually tuning inter- and intramolecular interactions, which are beneficial to the improvement of charge mobility.[10-13] Among the reported molecular systems, functionalized BDF derivatives with a donor-acceptor (D-A) structure are of prime importance to achieve high-performance organic electronic devices[1-4] and obtain dual-function molecular materials displaying both emissive and semiconducting properties.[9, 14]

Within the context of OLEDs, D-A-D type triads consisting of an anthraquinone (AQ) acceptor and triphenyl amine (TPA) donors are of particular interest as efficient red thermally activated delayed fluorescence (TADF) emitters.[15, 16] Both TPA and AQ are not only incorporated into photosensitizers for long-lived charge separation,[17-21] but also used as D and A subunits, respectively, for ambipolar materials in organic electronics,[22] electrochromic and gas separation applications.[23] In this paper, we describe the synthesis, characterization and electronic properties of a series of BDF-based triads either with an A-D-A or a D'-D-A structure by symmetrical coupling of electron acceptors, AQ and 11,11,12,12-tetracyano-9,10-anthraquinodimethane (TCAQ), or asymmetrical coupling of the electron donor TPA and AQ or TCAQ to a central BDF unit *via* ethylenic linkers (Scheme 1). Compared to analogous systems containing TPA and AQ/TCAQ,[15-17, 22-24] the introduction of vinyl linkers results in efficient π-conjugation between these redox-active subunits that extends over the entire planar system. Consequently, all of the triads strongly absorb in the visible spectral region due to an intramolecular charge transfer (ICT) from the BDF to AQ or TCAQ moieties. Herein we report a detailed study on ICT dynamics by ultrafast transient absorption spectroscopy techniques in combination with electrochemical and spectroelectrochemical data. The influence of electron-acceptor strength on the electronic properties of these triads is also demonstrated.

Results and Discussion

Synthesis and characterization

The synthetic routes to the target triads are outlined in Scheme 1. Starting from 2,6-bis(*N*,*N*-dihexylamino)-4,8-diiodobenzo[1,2-*b*:4,5-*b'*]difuran-3,7-dicarbonitrile (BDF-I), a palladium-catalyzed Heck cross-coupling reaction with 3 equivalents of 2-vinylanthracene-9,10-dione was accomplished to afford BDF-AQ and AQ-BDF-AQ in 31% and 59% yield, respectively. The subsequent Knoevenagel condensations with malononitrile, mediated by the Lehnert reagent $TiCl_4$ / pyridine lead to the formation of BDF-TCAQ and TCAQ-BDF-TCAQ in 96% and 60% yield, respectively. Similarly, the asymmetrically functionalized triad TPA-BDF-AQ was prepared *via* a palladium-catalyzed Heck cross-coupling reaction with *N*-phenyl-*N*-(4-vinylphenyl)aniline in 60% yield. The subsequent transformation to TPA-BDF-TCAQ was achieved by Knoevenagel condensation under the same condition for the symmetrically functionalized triad TCAQ-BDF-TCAQ

10.1002/hlca.202100099

although the yield is quite poor (10%). All of these new dyads and triads have been characterized by ^{1}H NMR and Mass spectrometry.

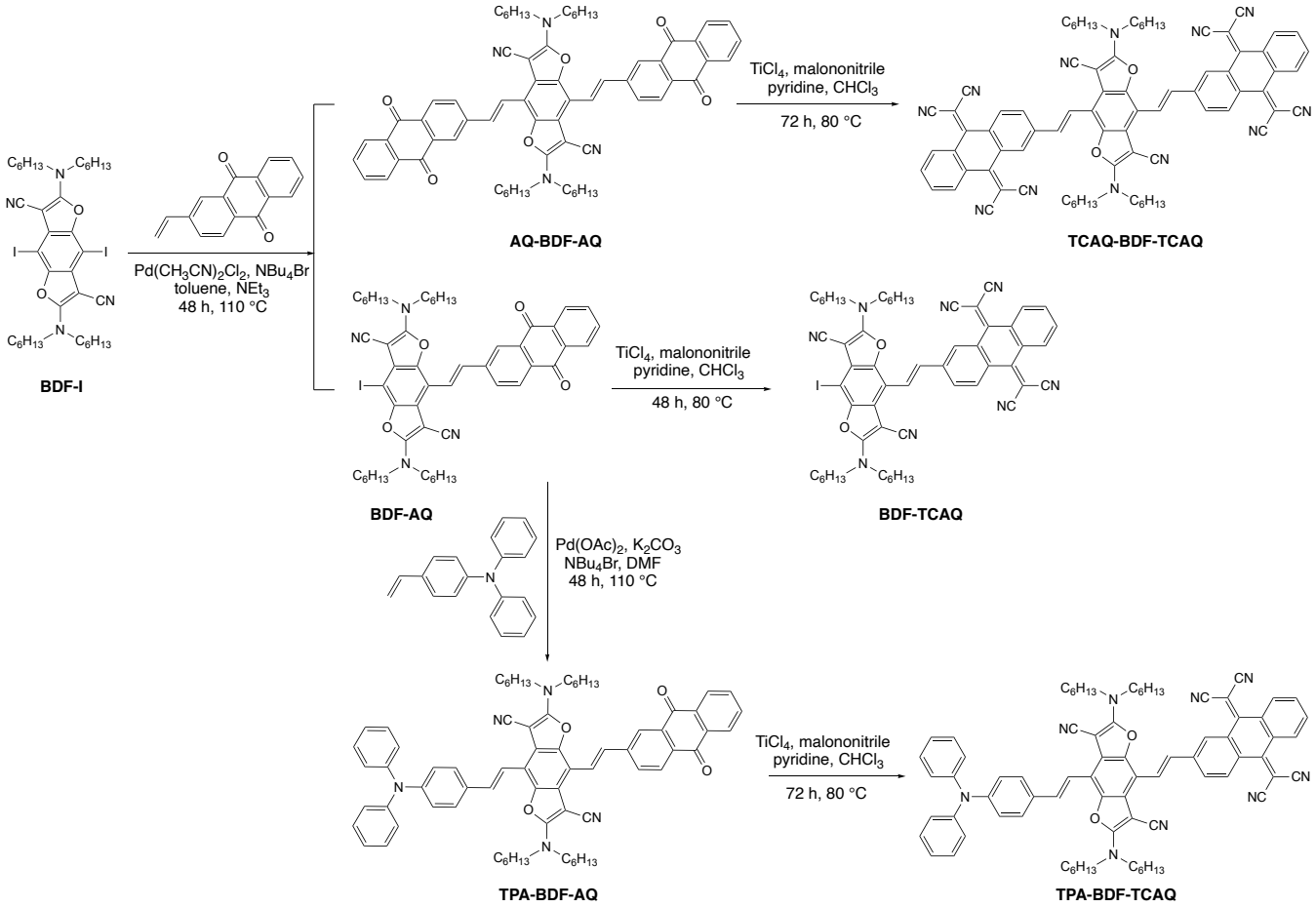

Scheme 1. Synthetic routes to the target compounds

Electrochemistry

Figure 1 shows the cyclic voltammograms of the four triads in CH_2Cl_2 at concentrations of around 10^{-5} M against an Ag/AgCl reference electrode in 0.1 M $TBAPF_6$ as supporting electrolyte. Table 1 summarizes their oxidation and reduction potentials together with those of the two dyads, as well as their electrochemical HOMO-LUMO gaps in terms of the difference between the first oxidation and the first reduction potentials.

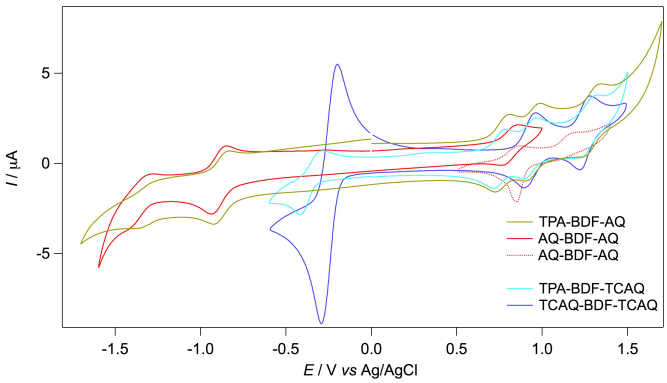

Figure 1. Cyclic voltammograms of AQ-BDF-AQ, TCAQ-BDF-TCAQ, TPA-BDF-AQ, and TPA-BDF-TCAQ in CH_2Cl_2 against an Ag/AgCl reference electrode.

As depicted in Figure 1, triad TCAQ-BDF-TCAQ undergoes two distinct, reversible single-electron oxidation processes and one reversible four-electron reduction, while AQ-BDF-AQ shows one reversible and one irreversible oxidation wave and two reversible reduction waves. The oxidation steps are clearly due to the removal of electrons localized on the BDF moiety, whereas the reduction steps correspond to sequential addition of electrons to the respective acceptor moieties. This is supported by the DFT calculations discussed below. As expected, replacement of AQ with a stronger acceptor TCAQ leads to a significant anodic shift in both oxidation and reduction potentials. Unlike the AQ moieties, the two TCAQ cores are reduced simultaneously to $TCAQ^{2-}$,[25] very probably due to the lack of effective electronic communication between them caused by a nonplanar butterfly-shape of TCAQ. For the asymmetric triads TPA-BDF-AQ and TPA-BDF-TCAQ, three reversible single-electron oxidation waves appear at very similar potentials. It seems likely that the electron-withdrawing effect of the acceptor core only has a negligible influence on the oxidation potentials of the TPA and BDF moieties. It can therefore be deduced that the TPA subunit, which is spatially distant from the acceptor core, is oxidized first. On the basis of simple electrostatic arguments, two subsequent oxidation processes of the BDF subunit occur at more positive potentials compared to the corresponding precursors BDF-AQ and BDF-TCAQ (Table 1). These

results are in good agreement with the sequence of oxidation steps confirmed by spectroelectrochemical measurements as shown in the following. Similar to the symmetric triads, TPA-BDF-AQ undergoes two reversible reduction processes, which are slightly shifted to positive potentials compared to BDF-AQ, while TPA-BDF-TCAQ reveals one reversible reduction wave which remains unchanged compared to BDF-TCAQ. This observation can presumably be accounted for by the fact that the planar AQ imparts stronger electronic communication between redox units *via* π-extended conjugation over the entire rigid and planar molecular backbone, which however does not hold for the nonplanar butterfly-shaped TCAQ.

Table 1. Redox potentials (*V* versus Ag/AgCl), onset oxidation and reduction potentials, ionization potentials (IP), electron affinities (EA), and electrochemical band gap E_g^{el} of the compounds measured in CH_2Cl_2.

Compound	$E_{1/2}^{ox1}$	$E_{1/2}^{ox2}$	$E_{1/2}^{ox3}$	E_{onset}^{ox1}	$E_{1/2}^{red1}$	$E_{1/2}^{red2}$	E_{onset}^{red1}	IP (eV)[b]	EA (eV)[c]	E_g^{el} (eV / cm^{-1})
BDF-AQ	0.75	1.09		0.65	-1.00	-1.46	-0.91	-4.96	-3.40	1.56 / 12580
TPA-BDF-AQ	0.77	0.95	1.29	0.68	-0.88	-1.32	-0.78	-4.99	-3.53	1.46 / 11775
AQ-BDF-AQ	0.81	1.20[a]		0.73	-0.89	-1.35	-0.79	-5.04	-3.52	1.52 / 12260
BDF-TCAQ	0.89	1.23		0.81	-0.31		-0.25	-5.12	-4.06	1.06 / 8550
TPA-BDF-TCAQ	0.75	0.93	1.27	0.70	-0.35		-0.32	-5.01	-3.99	1.02 / 8225
TCAQ-BDF-TCAQ	0.93	1.25		0.84	-0.25		-0.17	-5.15	-4.14	1.01 / 8145

[a] Irreversible peak. [b] Estimated from the onset oxidation potentials using empirical equations: IP = -(E_{onset}^{ox1} – 0.49 + 4.8) eV. [c] Estimated from the onset reduction potentials using empirical equations: EA = -(E_{onset}^{red1} – 0.49 + 4.8) eV.

Absorption spectroscopy

Figure 2 shows the UV-Vis absorption spectra of the two symmetric A-D-A triads TCAQ-BDF-TCAQ and AQ-BDF-AQ as well as the two asymmetric D'-D-A triads TPA-BDF-AQ and TPA-BDF-TCAQ in CH_2Cl_2 at concentrations of 2×10^{-5} M. None of the four compounds shows any luminescence at room temperature in CH_2Cl_2 solution, this implies that the well-known intense luminescence from the BDF moiety[9, 13, 26-29] is totally quenched. As will be discussed below, this quenching is most likely due to oxidative quenching with AQ or TCAQ acting as electron acceptors.

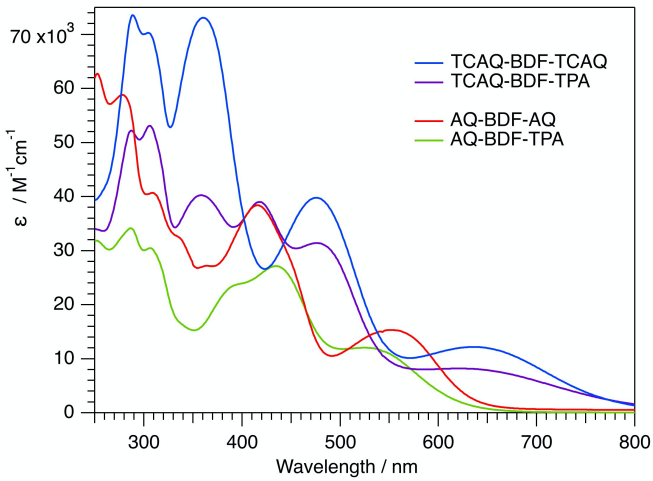

Figure 2. UV-Vis absorption spectra of AQ-BDF-AQ, TCAQ-BDF-TCAQ, TPA-BDF-AQ and TPA-BDF-TCAQ in CH_2Cl_2 at room temperature ($c = 2\times10^{-5}$ M).

For AQ-BDF-AQ, the lowest energy absorption band is centered at 560 nm (17800 cm^{-1}), that is at much lower in energy than any of the absorption bands of the constituting moieties.[13, 30] The same holds for TCAQ-BDF-TCAQ, for which the lowest energy band is at even lower energy, that is, centered at 650 nm (15400 cm^{-1}). For the mixed triads, the lowest energy transitions are at the same energies as for the symmetric triads of the corresponding acceptor moieties, but with only around half the intensities. This indicates that the lowest energy electronic excitations correspond to intramolecular charge transfer (ICT) transitions from BDF to AQ and TCAQ, respectively. This is in line with DFT calculations as illustrated in Figure 3 for AQ-BDF-AQ, for which the $S_0 \rightarrow S_1$ transition, calculated at 625 nm (16000 cm^{-1}), recognizably corresponds to an ICT from the HOMO which is fully localized on the BDF unit to the LUMO localized on the AQ moieties. Also, higher energy transitions, in particular the second intense band at 455 nm (22000 cm^{-1}), correspond to ICT transitions (see Figure S1 of the SI for more details).

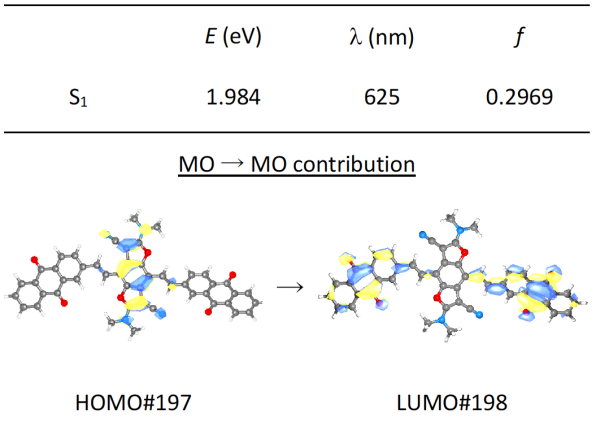

Figure 3. Results of DFT calculations for AQ-BDF-AQ showing the HOMO and the LUMO and the associated $S_0 \rightarrow S_1$ transition with a >99% contribution of the two MOs. For full results of the calculations see Figure S1 of the SI.

The above also holds for TCAQ-BDF-TCAQ, whereby the cyano groups essentially stabilize the LUMO by around 0.6 eV. For the TPA containing

triads, the HOMO is in delocalized over both the BDF and the TPA moieties (see Figure S2 of the SI for DFT results on TPA-BDF-AQ). But as surmised above the lowest energy transition is still an ICT transition comprising AQ and TCAQ as acceptors.

The experimental value of 562 nm (17800 cm^{-1}) for the lowest-energy ICT transition of the AQ-BDF-AQ triad corresponds to the optical HOMO-LUMO gap of the unrelaxed species. In order to compare it to the electrochemical HOMO-LUMO gap of 1.52 eV (Table 1), the zero-point energy difference has to be taken. In the absence of any luminescence this has to be estimated from the onset of the absorption at approximately 650 nm or 15000 cm^{-1} (1.85 eV). Due to electron-electron repulsion, the value of the optical gap is somewhat larger than the electrochemical value reported in Table 1, but it is nevertheless of the right order to further substantiate the assignment of the lowest energy absorption band to an ICT transition.

Spectroelectrochemistry

In order to shed more light on the photophysical behavior of the series of triads, spectroelectrochemical measurements were performed in a thin layer cell using a Ag wire pseudo reference electrode. For details see the experimental section. Figure 4a shows the evolution of the absorption spectrum of AQ-BDF-AQ in the oxidizing mode upon application of a positive potential of 1000 mV. According to its CV data, this is sufficient to rapidly remove two electrons sequentially from the BDF moiety. In a first step and within the first 40 s the ICT band at 555 nm disappears and new band structures at around 525 nm and between 800 and 1050 nm appear. Upon prolonged application of this potential, the band structure in the near IR disappears again, but at the same time the overall intensity of the observed transitions drops, indicating that this second step is non-reversible, in agreement with the CV data. The spectrum after 40 s is thus due to a species with one electron removed from the HOMO, best described as AQ-BDF$^{\bullet+}$-AQ. The band at 525 nm is due to the ICT transition from the SOMO still localized on the BDF unit to the same LUMO as before, now at slightly higher energy than before oxidation due to the stabilization of the SOMO with respect to the HOMO of the neutral species. The band structure in the NIR can tentatively be attributed to a series of SOMO-x $\rightarrow$ SOMO transitions localized on the BDF$^{\bullet+}$ moiety, as there is no other low-energy MO available for an absorption in this energy range (see Figure S1 of the SI).

Figure 4b shows the evolution of the absorption spectrum of AQ-BDF-AQ in the reducing mode upon application of a negative potential of -1200 mV. At this potential, the two AQ moieties are sequentially reduced to AQ$^{\bullet-}$ as is evident from the evolution of the spectrum in two steps, that is, a fairly rapid change in the spectrum within the first 800 s, followed by a slower change leading to a stable final species within 2800 s (see Figure S3 of the SI). Thus, the resulting species are best described as AQ-BDF-AQ$^{\bullet-}$ after the first step and AQ$^{\bullet-}$-BDF-AQ$^{\bullet-}$ for the final species. In principle the species after the first step is a mixed valence species. Even though the LUMO of the neutral species is delocalized over both AQ moieties, upon the first reduction, the unpaired electron is in all probability quickly localized on one of the AQ acceptor moieties due to the interaction with the moderately polar solvent making it at most a class II mixed valence system.[31] As a result, the BDF to AQ ICT band now only involving the still neutral moiety moves to slightly higher energy and loses intensity. The final species after prolonged reduction has intense absorption bands at 380 nm and 480 nm, characteristic of AQ$^{\bullet-}$,[32] and a very broad and comparatively weak band in the region of 1100 nm, which can tentatively be attributed to aggregates of AQ$^{\bullet-}$-BDF-AQ$^{\bullet-}$ triggered by π-extended conjugation over the entire rigid and planar molecular backbone. The nature of the band structure from 600 - 700 nm is not straightforward to attribute.

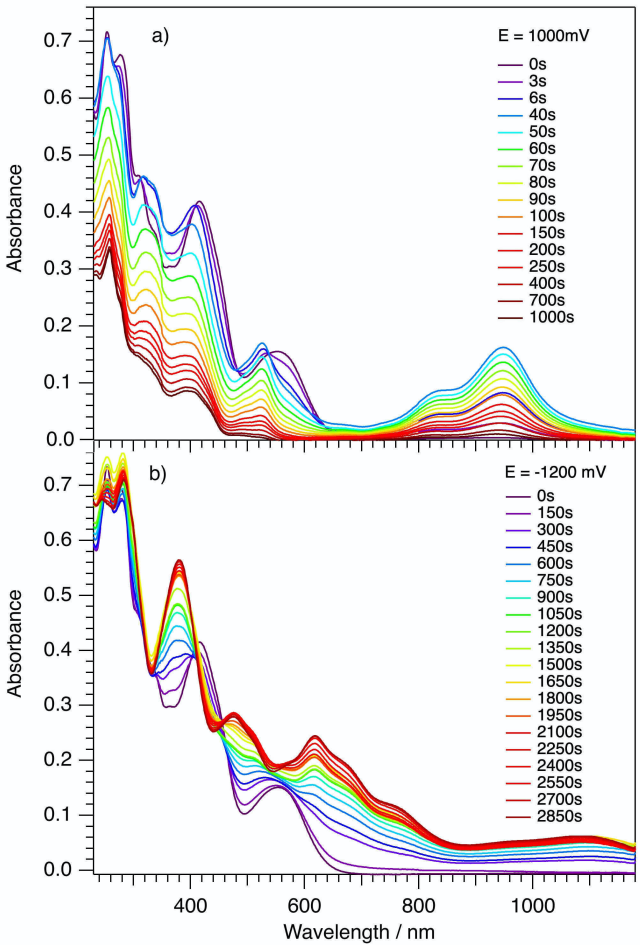

Figure 4. Evolution of the UV-Vis absorption spectrum of AQ-BDF-AQ upon application of a positive voltage of 1000 mV (a) and a negative voltage of -1200 mV (b) against an Ag wire pseudo reference electrode in the spectroelectrochemical cell at a concentration of 2×10^{-4} M in CH_2Cl_2.

Figure 5 shows the spectroelectrochemical evolution of the absorption spectra of the mixed triad TPA-BDF-AQ in reductive and oxidative modes. In the oxidative mode at 850 mV (Figure 5a) the oxidation occurs in two steps, whereby the first step is comparatively rapid and results in a spectrum with a strong broad band centered at 1550 nm (blue curve). As for the previously published data on the symmetric triad TPA-BDF-TPA,[33] the first oxidation step results in the removal of an electron from the TPA unit resulting in a species best described as TPA$^{\bullet+}$-BDF-AQ. Thus, the band at 1550 nm corresponds to a BDF to TPA$^{\bullet+}$ ICT transition. Upon prolonged oxidation, this band disappears again. This is due to the second oxidation step removing an

electron more localized on the BDF unit. The nature of the intense band appearing at 750 nm is not easy to define, but it is reminiscent of the published spectrochemical spectrum of TPA-BDF-TPA of the third oxidative step. In stark contrast to AQ-BDF-AQ, the ICT band at 555 nm gradually decreases without moving to slightly higher energy in the spectra of the reduction of TPA-BDF-AQ at -1350 mV, leading to clear isosbestic points. This observation indicates that this is a clean one electron process involving only two species. As the LUMO is fully localized on the AQ moiety (see Figure S2 in the SI), the resulting species has best been described as TPA-BDF-AQ$^{\bullet-}$. As for the symmetric triad the resulting band structure is not straightforward to attribute.

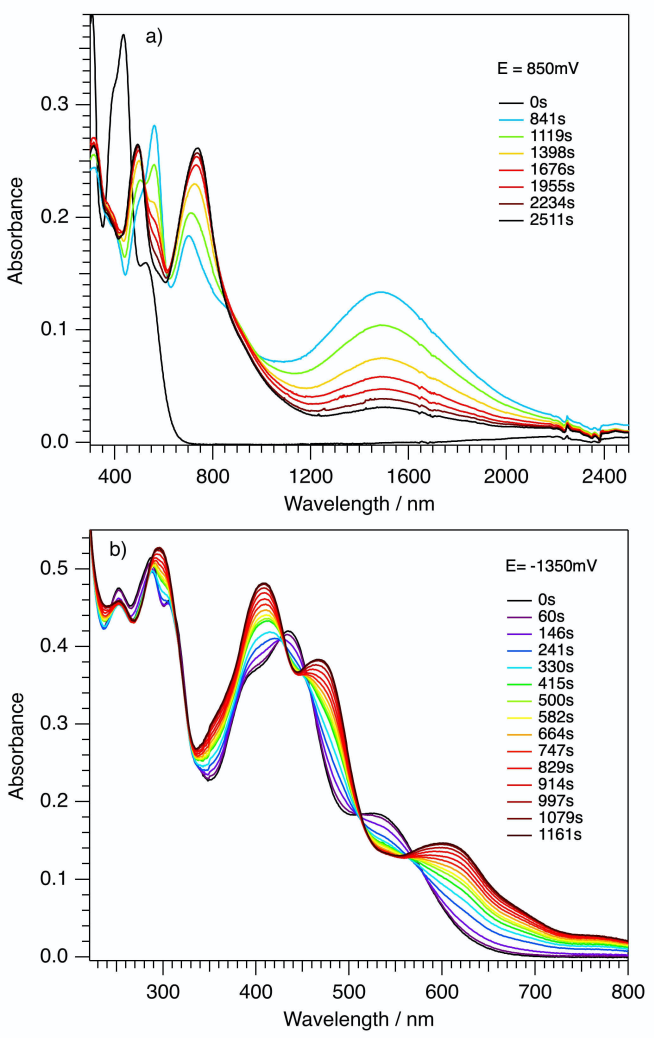

Figure 5. Evolution of the UV-Vis absorption spectrum of TPA-BDF-AQ upon application of a positive voltage of 850 mV (a) and a negative voltage of -1350 mV (b) against an Ag wire pseudo reference electrode in the spectroelectrochemical cell at a concentration of 2×10^{-4} M in CH_2Cl_2.

The results of spectrochemical measurements on TCAQ-BDF-TCAQ and TPA-BDF-TCAQ are shown in Figures S4 and S5 of the SI. They are in line with the results for the two compounds with AQ as substituents, except that, as TCAQ is a somewhat better acceptor than AQ, the reduction occurs at a much less negative potential.

Ultrafast optical spectroscopy

In order to shed more light on the electronic structure and the photophysical properties of the four triads, ultrafast optical spectroscopy experiments were performed. Figure 6a shows the evolution of the difference spectrum of TCAQ-BDF-TCAQ in THF as a function of delay time following pulsed excitation at 400 nm. The early spectrum appearing within the instrumental response function (IRF) of the set-up, that is, at t < 0.5 ps, exhibits a pronounced bleaching of the ground state band at 460 nm and a strong absorption centered at 600 nm. The spectrum subsequently evolves very rapidly (see Figure S6 in the SI). The transient absorption (TA) data were analysed globally assuming a series of successive exponential steps. A good fit was obtained assuming three successive steps with $\tau_1 \approx \tau_2 = 0.55$ ps and $\tau_3 = 2.5$ ps and the species-associated difference absorption spectra (SADS) shown in Figure 6b. The first two SADS are quite similar and, therefore, the A→B step most probably corresponds to relaxation of the Franck-Condon excited state and SADS of A and B to the unrelaxed and relaxed initially excited state TCAQ-BDF-TCAQ*, respectively, which are in principle delocalized over the two TCAQ moieties. C can be associated with the charge-separated state with the electron driven to one of the TCAQ moieties, TCAQ-BDF^{+}TCAQ^{-} by the interaction with the solvent,[34-38] that is, charge separation occurs on a timescale of 0.55 ps. The charge separated state then recombines to the ground state within 2.5 ps. Given the timescale of these processes, non-exponential dynamics can be expected and, thus, the SADS cannot strictly be attributed to a given state or species and should rather be considered as evolution-associated difference spectra. Similarly, the time constants should not be over-interpreted but should only be considered as indication of the main timescales.

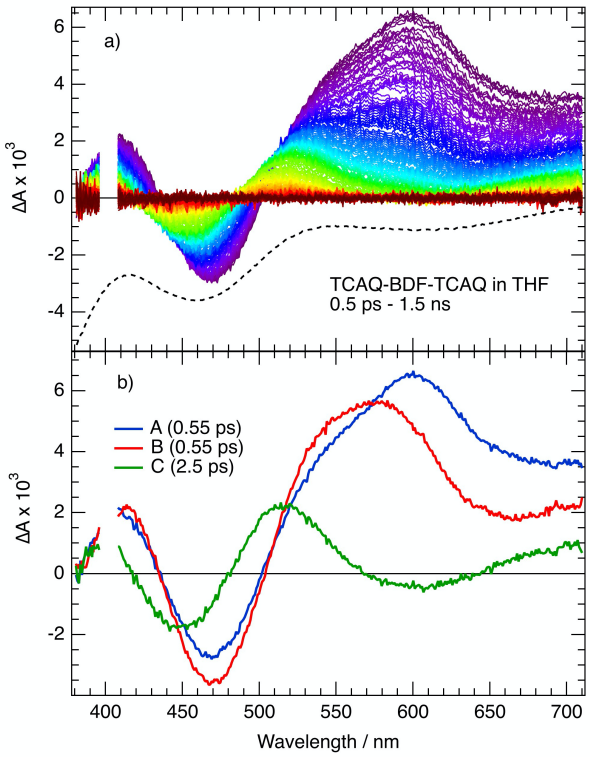

Figure 6. a) Transient absorption spectra measured at different time delays after 400 nm excitation of TCAQ-BDF-TCAQ in THF, the black line is the

negative ground state absorption, b) SADS obtained from a global analysis assuming a series of three successive steps $A \xrightarrow{-\tau_1} B \xrightarrow{-\tau_2} C \xrightarrow{-\tau_3} GS$, with $\tau_1 \approx \tau_2 = 0.55$ ps, and $\tau_3 = 2.5$ ps.

As a further point of interest, the SADS of species C corresponds quite well with the difference spectrum of the first electrochemical reduction step, with increased absorptions above 650 and below 425 nm and centered at 525 nm, and bleaching centered at 600 and 475 nm (compare with Figure S4 of the SI), as further indication of the presence of a $TCAQ^{\bullet-}$ moiety.

The behavior of the asymmetric triad TPA-BDF-TCAQ is very similar to the one of the symmetric one with two TCAQ substituents, and can be analyzed using the same relaxation scheme with two very fast and one somewhat slower process also with a time constant of around 2.5 ps (see Figure S7 of the SI for details). It may be concluded that TPA does not significantly participate in the relaxation processes following excitation at 400 nm.

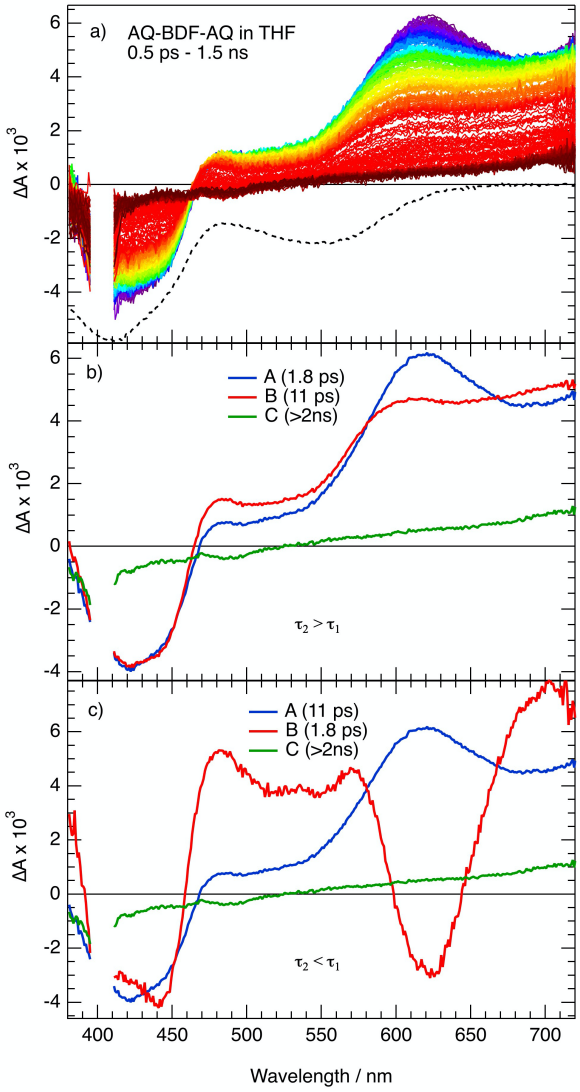

Figure 7. a) Transient absorption spectra measured at different time delays after 400 nm excitation AQ-BDF-AQ in THF, the black line is the negative ground state absorption, b) SADS assuming $A \xrightarrow{-\tau_1} B \xrightarrow{-\tau_2} GS$, c) SADS with the inverted target analysis $A \xrightarrow{-\tau_2} B \xrightarrow{-\tau_1} GS$; for both $\tau_1 = 1.8$ ps, and $\tau_2 = 11$ ps.

Figure 7a shows the transient absorption spectra measured with the triad AQ-BDF-AQ. As for the TCAQ derivatives, the spectrum appearing within the IRF of the experimental set-up shows a bleaching of the higher energy ICT band of the ground state and an excited state absorption at around 625 nm, but in contrast to these, this spectrum evolves comparatively little within the first 2 ps. From there the intensity decays to a residual small background within 40 ps. Neglecting this background, either due to photochemical degradation or possible ultrafast intersystem crossing in AQ,[39] the time evolution can be reproduced assuming two exponential steps with $\tau_1 = 1.8$ ps and $\tau_2 = 11$ ps, and the corresponding decay associated difference spectra are shown in Figure S8 of the SI.

Target analysis and its interpretation are not straightforward. Assuming an $A \xrightarrow{-\tau_1} B \xrightarrow{-\tau_2} GS$ kinetic scheme results in the SADS shown in Figure 7b. It is tempting to simply attribute species A and B to the unrelaxed and relaxed initially excited state. However, in view of the results for the TCAQ derivative, the value of $\tau_1 = 1.8$ ps for the initial relaxation seems very long indeed. Also, the relaxed initial state would then have lifetime of $\tau_2 = 11$ ps and relax straight to the ground state. Again, this is in contradiction to the results for the TCAQ derivative. Alternatively, charge separation could be faster than the IRF, so that species A and B correspond to the unrelaxed and relaxed charge separated state. This state would then have a lifetime of τ_2. However, the spectral features of species B in this scenario do not in any way resemble the spectral features of species C of the TCAQ derivative in Figure 6b.

A third possibility is that charge separation in AQ-BDF-AQ is not ultrafast and slower than charge recombination. To explore this possibility, the target analysis was performed with inverted kinetics, that is $A \xrightarrow{-\tau_2} B \xrightarrow{-\tau_1} GS$. The SADS of species A is very similar to the one of species A of the first relaxation scheme and also similar to the one of species A and B of the TCQA derivative. It can thus be attributed to the relaxed initially excited state, AQ-BDF-AQ*, populated within the IRF of the set-up. But the SADS of species B is now very different, with bleaching around 425 and 625 nm and excited state absorptions between 460 and 600 and above 650 nm. This is reminiscent of the SADS of species C in the TCAQ derivative, which was attributed to a charge separated state. In view of the similarities between the SADS of the TCAQ derivative and the SADS for AQ-BDF-AQ, the inverse kinetic scheme with species C as $AQ\text{-}BDF^{+}\text{-}AQ^{-}$, is very plausible. It is important to note that the absence of strong features related to the charge separated state in the transient absorption spectra is due to the fact that charge recombination occurs faster than charge separation. Because of this, the population of the charge separated state never accumulates enough to be clearly visible. The transient absorption spectra and the corresponding analysis for the mixed triad TPA-BDF-AQ (see Figures S9 and S10 of the SI) corroborate the results found for AQ-BDF-AQ and confirm that TPA plays a negligible role in the photophysical properties of the mixed triads. Apparently TPA is not a strong enough donor compared to BDF for hole transfer from BDF to TPA to compete with charge recombination.

The actual values of the time constants for charge separation and charge recombination for the two systems require further discussion. Figure 8 may serve to illustrate these. For TCAQ the relaxation of the initially excited state

is only just discernible, being only slightly slower than the IRF of the experimental set-up. For AQ as this process occurs within the IRF. For TCAQ as acceptor the charge separation occurs within 0.55 ps, for AQ as acceptor it takes 11 ps. As TCAQ is a substantially better acceptor than AQ, and as for this process we are in the Marcus normal region, the substantially faster charge separation for TCAQ is expected. The charge recombination, on the other hand is expected to be in the Marcus inverted region, in which the process should likewise be slower for the AQ systems. Experimentally, the values for the two acceptors are very close to each other, and for both the dynamics are ultrafast and occur at least partially out of equilibrium. Consequently, this theoretical model loses, at least partially, its validity. Moreover, differences in other parameters such as the electronic and vibronic coupling should also be considered.

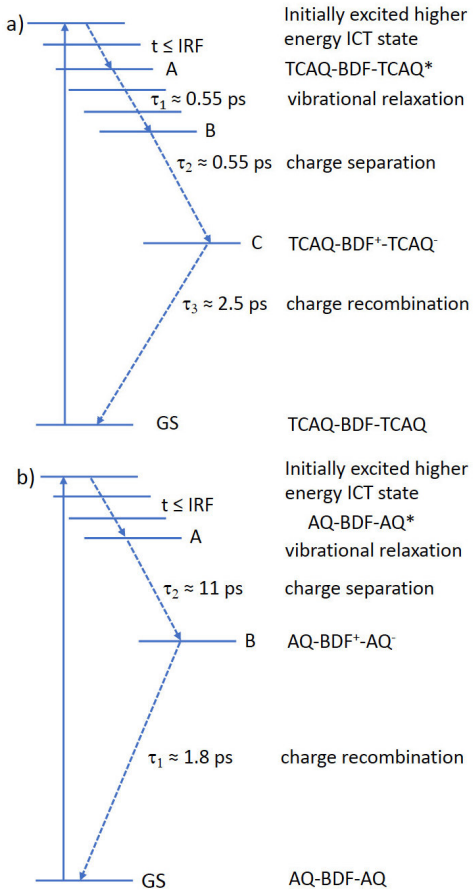

Figure 8. Schematic representation of the relaxation processes for a) TCAQ-BDF-TCAQ with A: initially excited state during relaxation, B: relaxed initial state, C: charge separated state, and b) AQ-BDF-AQ with A: relaxed initially excited state, B: charge separated state; GS: ground state.

Conclusions

A fundamental understanding of electronic interactions between specific electroactive chromophores and optical properties of their combinations is of high interest in the development of novel organic materials for applications in molecular (opto)electronics. Consequently, a series of BDF-based D-π-A conjugates has been synthesized and characterized. All of the triads and dyads have a perfectly planar structure of the central molecular core consisting of D and A components linked by vinyl groups, leading to an effective π-extended conjugation. The triads and dyads undergo several redox processes and strongly absorb in the visible spectral region because of ICT from the HOMO localized on the BDF core to the LUMO localized on the corresponding acceptors such as AQ and TCAQ. The intricate charge transfer dynamics has been investigated by ultrafast transient absorption spectroscopy. In combination with electrochemical and spectroelectrochemical data, the charge separation and recombination processes have been analyzed and the kinetic schemes were discussed in order to rationalize the lack of long-lived highly energetic charge separation states. For the symmetric A-D-A triads, the negative charge of the ICT state is actually localized on one of the acceptor moieties, but as the donor and the acceptor are spatially so close to each other, a rapid charge recombination occurs within a few ps. For the asymmetric systems, the positive charge of the ICT state is distributed over both the TPA and the BDF units, which renders charge recombination quite rapid. As a consequence, in further experiments TPA will be replaced with a much stronger donor unit, or other aromatic bridges will be chosen to increase the D/A separation distance, such that the positive and the negative charges of the ICT state become truly separated. Hence, further studies with a greater diversity of D-π-A conjugated systems will be indispensable to elucidate the crucial factors for enhancing the lifetime of a potential intramolecular charge separation.

Experimental Section

Materials and methods

2,6-Bis(N,N-dihexylamino)-4,8-diiodobenzo[1,2-*b*:4,5-*b'*] difuran-3,7-dicarbonitrile, *N*-phenyl-*N*-(4-vinylphenyl)aniline, and 2-vinylanthracene-9,10-dione were synthesized according to the literature procedures. All chemicals and solvents were purchased from commercial sources and were used without further purification. All reactions were carried out, unless mentioned, under normal laboratory conditions in air.

All ^{1}H NMR spectra were measured at 300 MHz. Chemical shifts (δ) were calibrated against the solvent as an internal standard. The chemical shift δ is given in ppm and the following abbreviations are used: s for singlet, d for doublet, t for triplet and m for multiplet. Mass spectra were recorded, unless mentioned, with an LTQ Orbitrap XL spectrometer for the ESI ionisation mode.

The cyclic voltammetry (CV) measurements were performed and recorded with a Metrohm 663 VA Stand apparatus. A Pt-electrode was used as working electrode and a glassy carbon electrode as a counter electrode. An Ag/AgCl electrode was used as a reference electrode and a 0.1 M solution of tetrabutylammonium-hexafluorophosphate (Bu_4NPF_6) in CH_2Cl_2 (Acros Organics, for HPLC) was used as supporting electrolyte.

High quality absorption spectra of all compounds in CH_2Cl_2 were recorded with a Cary 5000 dual beam spectrometer at concentrations of 2×10^{-5} M in 1 cm quartz cells. Spectroelectrochemical measurement were performed at concentrations of 2×10^{-4} M in the same solvent with 0.1 M Bu_4NPF_6 as supporting electrolyte using an optically transparent thin layer cell (d = 0.7

mm) from Specac placed inside the Cary 5000 spectrometer. The electrochemical potential was applied by using a potentiostat in three-electrode configuration, with platinum working and counter electrodes. All potentials are given versus a silver wire pseudo-reference electrode. The difference between the silver wire pseudo-reference and the Ag/AgCl electrodes is less than 100 mV.

The TA measurements have been carried out with the transient absorption (TA) setup described in previously reported work.[40, 41] The fluence of the 400 nm pump pulses on the sample was ca. 1 mJ cm^{-2}. A white light continuum (between 360 nm and 750 nm) was used for probing. The polarization of the probe pulses relative to that of the pump pulse was at magic angle. All spectra were corrected for the chirp of the white-light continuum. The instrument response function (IRF) the setup was around 150 fs (full width at half maximum). The samples were located in a 1 mm quartz cell and bubbled continuously by N2 during all measurements. The absorbance of the samples at 400 nm was between 0.1 and 0.2 in THF.

DFT calculations have been performed with the B3LYP functional[42, 43] and the DZVP2 basis set[44] using the NWChem program package.[45] The optimization calculations were performed using tight convergence criteria and the subsequent TDDFT electronic calculations were performed within the Tamm-Dancoff approximation.[46, 47]

Synthetic procedures

BDF-AQ and AQ-BDF-AQ: A mixture of **BDF-I** (329.4 mg, 0.398 mmol), 2-vinylanthracene-9,10-dione (280 mg, 1.19 mmol), toluene (30 mL), NBu_4Br (384.6 mg, 1.19 mmol), $Pd(MeCN)_2Cl_2$ (31 mg, 0.119 mmol) and NEt_3 (2 mL) was bubbled with N_2 for 10 min. The resulting solution was heated at 110 °C for 48 h in an inert atmosphere. The solvent was evaporated by rotavapor and the residue was subjected to column chromatography on silica gel, eluting with a gradient of CH_2Cl_2 and EtOAc (1:0 to 9:1) to afford a red **BDF-AQ** (115 mg, 31%) and a dark red product **AQ-BDF-AQ** (245 mg, 59%).

BDF-AQ: ^{1}H NMR (300 MHz, $CDCl_3$) δ 8.34-8.30 (m, 4H), 8.15 (d, *J* = 16.3 Hz, 1H), 8.04 (dd, *J* = 8.2, 1.6 Hz, 1H), 7.82-7.79 (m, 2H), 7.57 (d, *J* = 16.3 Hz, 1H), 3.71-3.60 (m, 8H), 1.87-1.73 (m, 8H), 1.51-1.28 (m, 24H), 0.97-0.77 (m, 12H).

ESI-MS: Calc. for $[C_{52}H_{61}IN_4O_4]$ 932.37 found 932.02.

AQ-BDF-AQ: ^{1}H NMR (300 MHz, $CDCl_3$) δ 8.32-8.28 (m, 8H), 8.19 (d, *J* = 16.3 Hz, 2H), 8.04 (dd, *J* = 8.3, 1.7 Hz, 2H), 7.74 (dd, *J* = 5.8, 3.3 Hz, 4H), 7.58 (d, *J* = 16.5 Hz, 2H), 3.75-3.70 (m, 8H), 1.90-1.82 (m, 8H), 1.43-1.30 (m, 24H), 0.95-0.81 (m, 12H).

ESI-MS: Calc. for $[C_{68}H_{70}N_4O_6]$ 1038.53 found 1038.416.

TPA-BDF-AQ: A mixture of **BDF-AQ** (252 mg, 0.27 mmol), *N*-phenyl-*N*-(4-vinylphenyl)aniline (95.2 mg, 0.35 mmol), K_2CO_3 (55.4 mg, 0.405 mmol), NBu_4Br (87 mg, 0.27 mmol), $Pd(OAc)_2$ (12.12 mg, 0.054 mmol) and DMF (20 mL) was bubbled with N_2 for 10 min. The resulting solution was heated at 110 °C for 48 h in an inert atmosphere. The solvent was evaporated by rotavapor and the residue was subjected to column chromatography on silica gel, eluting with a gradient of CH_2Cl_2 and hexane (1:1 to 1:0) to afford a red crystalline product **TPA-BDF-AQ** (175 mg, 60%).

^{1}H NMR (300 MHz, $CDCl_3$) δ 8.30-8.22 (m, 5H), 8.02 (dd, *J* = 8.2, 1.7 Hz, 1H), 7.83 (d, *J* = 16.3 Hz, 1H), 7.79-7.76 (m, 2H), 7.55 (d, *J* = 16.1 Hz, 1H), 7.40 (dd, *J* = 12.4, 9.0 Hz, 3H), 7.29-7.24 (m, 4H), 7.13-7.11 (m, 4H), 7.06-7.02 (m, 4H), 3.72-3.63 (m, 8H), 1.85-1.80 (m, 8H), 1.47-1.35 (m, 24H), 0.87 (td, *J* = 7.0, 2.8 Hz, 12H).

ESI-MS: Calc. for $[C_{72}H_{77}N_5O_4]$ 1075.60 found 1075.60.

BDF-TCAQ: Malononitrile (21.2 mg, 0.322 mmol), $TiCl_4$ (60.9 mg, 0.322 mmol), and pyridine (50.8 mg, 0.64 mmol) were added to **BDF-AQ** (100 mg, 0.107 mmol) in $CHCl_3$ (30 mL). The reaction mixture was heated to reflux for 48 h. After every 12 h, identical amounts of malononitrile, $TiCl_4$, and pyridine were added. The resultant mixture was poured on ice/water and extracted with $CHCl_3$ (3 × 100 mL). The combined organic layer was dried over $MgSO_4$, concentrated in vacuo, washed with Et_2O to remove excess of malononitrile, and subjected to column chromatography on silica gel, eluting with a gradient of CH_2Cl_2 and hexane (3:1 to 1:0) to afford a dark red product **BDF-TCAQ** (117.1 mg, 96%).

^{1}H NMR (300 MHz, $CDCl_3$) δ 8.29-8.23 (m, 4H), 8.14 (d, *J* = 16.3 Hz, 1H), 7.88 (dd, *J* = 8.4, 1.4 Hz, 1H), 7.76-7.73 (m, 2H), 7.48 (d, *J* = 16.4 Hz, 1H), 3.78-3.54 (m, 8H), 1.88-1.67 (m, 8H), 1.42-1.25 (m, 24H), 0.98-0.75 (m, 12H).

ESI-MS: Calc. for $[C_{58}H_{61}IN_8O_2]$ 1028.40 found 1027.93.

TCAQ-BDF-TCAQ: Malononitrile (35.9 mg, 0.54 mmol), $TiCl_4$ (103.01 mg, 0.54 mmol), and pyridine (85.9 mg, 1.09 mmol) were added to **AQ-BDF-AQ** (94 mg, 0.091 mmol) in $CHCl_3$ (30 mL), and the mixture was heated to reflux for 72 h. After every 12 h, identical amounts of malononitrile, $TiCl_4$, and pyridine were added. The resultant mixture was poured on ice/water and extracted with $CHCl_3$ (3 × 100 mL). The combined organic phase was dried over $MgSO_4$, concentrated in vacuo, washed with Et_2O to remove excess of malononitrile, and subjected to column chromatography on silica gel, eluting with CH_2Cl_2 and EtOAc (50:1) to afford a dark green product **TCAQ-BDF-TCAQ** (67 mg, 60%).

^{1}H NMR (300 MHz, $CDCl_3$) δ 8.31-8.23 (m, 10H), 7.90 (dd, *J* = 8.4, 0.9 Hz, 2H), 7.76-7.73 (m, 4H), 7.53 (d, *J* = 16.2 Hz, 2H), 3.70 (t, *J* = 7.1 Hz, 8H), 1.88-1.78 (m, 8H), 1.48-1.28 (m, 24H), 0.89 (t, *J* = 6.9 Hz, 12H).

ESI-MS: Calc. for $[C_{80}H_{70}N_{12}O_2]$ 1230.57 found 1231.58.

TPA-BDF-TCAQ: Malononitrile (32.4 mg, 0.49 mmol), $TiCl_4$ (93 mg, 0.49 mmol), and pyridine (77.6 mg, 0.98 mmol) were added to **TPA-BDF-AQ** (175 mg, 0.16 mmol) in $CHCl_3$ (20 mL), and the reaction mixture was heated to reflux for 72 h. After every 24 h, identical amounts of malononitrile, $TiCl_4$, and pyridine were added. The resulting mixture was poured on ice/water and extracted with $CHCl_3$ (3 × 100 mL). The combined organic phase was dried over $MgSO_4$, concentrated in vacuo, washed with Et_2O to remove excess of malononitrile, and subjected to column chromatography on silica gel, eluting with CH_2Cl_2 and hexane (9:1) to afford a dark green product **TPA-BDF-TCAQ** (20 mg, 10.5%).

^{1}H NMR (300 MHz, CD_2Cl_2) δ 8.32-8.22 (m, 5H), 7.92-7.85 (m, 2H), 7.77-7.74 (m, 2H), 7.56-7.40 (m, 4H), 7.32-7.27 (m, 4H), 7.13-7.02 (m, 8H), 3.74-3.51 (m, 8H), 1.86-1.75 (m, 8H), 1.44-1.29 (m, 24H), 0.93-0.85 (m, 12H).

ESI-MS: Calc. for $[C_{78}H_{77}N_9O_2]$ 1171.62 found 1171.62.

Supplementary Material

Supporting information for this article is available on the WWW under http://dx.doi.org/10.1002/MS-number.

Acknowledgements

A. Hauser thanks the Department of physical chemistry of the University of Geneva for support.

Author Contribution Statement

S. Keller and S.-X- Liu synthesized the compounds, performed their analysis by NMR spectroscopy and electrochemistry. J. Hankache, Q. Sun and J. Ding performed the absorption and spectroelectrochemical experiments, O. Yushchenko and E. Vauthey performed the ultrafast spectroscopic experiments, and M. Lawson Daku performed the DFT calculations. A. Hauser and E. Vauthey developed the model for the interpretation of the spectroscopic data. S.-X. Liu, A. Hauser, S. Decurtins and R. Häner edited the manuscript.

References

[1] Y. Gao, Z. Shen, F. Tan, G. Yue, R. Liu, Z. Wang, S. Qu, Z. Wang, W. Zhang, 'Novel benzo[1,2-b:4,5-b']difuran-based copolymer enables efficient polymer solar cells with small energy loss and high VOC', *Nano Energy* **2020**, *76*, 104964.

[2] R. Zhu, Z. Wang, Y. Gao, Z. Zheng, F. Guo, S. Gao, K. Lu, L. Zhao, Y. Zhang, 'Chain Engineering of Benzodifuran-Based Wide-Bandgap Polymers for Efficient Non-Fullerene Polymer Solar Cells', *Macromol. Rapid Commun.* **2019**, *40*, 1900227.

[3] F. Wang, Y. Dai, W. Wang, H. Lu, L. Qiu, Y. Ding, G. Zhang, 'Incorporation of heteroatoms in conjugated polymers backbone toward air-stable, high-performance n-channel unencapsulated polymer transistors', *Chem. Mater.* **2018**, *30*, 5451-5459.

[4] H. Bin, L. Zhong, Y. Yang, L. Gao, H. Huang, C. Sun, X. Li, L. Xue, Z.-G. Zhang, Z. Zhang, Y. Li, 'Medium Bandgap Polymer Donor Based on Bi(trialkylsilylthienyl-benzo[1,2-b:4,5-b']-difuran) for High Performance Nonfullerene Polymer Solar Cells', *Adv. Energy Mater.* **2017**, *7*, 1700746.

[5] L. Huo, T. Liu, B. Fan, Z. Zhao, X. Sun, D. Wei, M. Yu, Y. Liu, Y. Sun, 'Organic Solar Cells Based on a 2D Benzo[1,2-b:4,5-b']difuran-Conjugated Polymer with High-Power Conversion Efficiency', *Adv. Mater.* **2015**, *27*, 6969-6975.

[6] J. Warnan, C. Cabanetos, A. El Labban, M. R. Hansen, C. Tassone, M. F. Toney, P. M. Beaujuge, 'Ordering Effects in Benzo[1,2-b:4,5-b']difuran-Thieno[3,4-c]pyrrole-4,6-dione Polymers with >7% Solar Cell Efficiency', *Adv. Mater.* **2014**, *26*, 4357-4362.

[7] C. Moussalem, O. Segut, F. Gohier, M. Allain, P. Frere, 'Facile Access via Green Procedures to a Material with the Benzodifuran Moiety for Organic Photovoltaics', *ACS Sustainable Chem. Eng.* **2014**, *2*, 1043-1048.

[8] B. Liu, X. Chen, Y. Zou, L. Xiao, X. Xu, Y. He, L. Li, Y. Li, 'Benzo[1,2-b:4,5-b']difuran-Based Donor-Acceptor Copolymers for Polymer Solar Cells', *Macromolecules* **2012**, *45*, 6898-6905.

[9] H. Tsuji, C. Mitsui, Y. Sato, E. Nakamura, 'Bis(carbazolyl)benzodifuran: A High-Mobility Ambipolar Material for Homojunction Organic Light-Emitting Diode Devices', *Adv. Mater.* **2009**, *21*, 3776-3779.

[10] C. Huang, S. Chen, K. Baruel Ornso, D. Reber, M. Baghernejad, Y. Fu, T. Wandlowski, S. Decurtins, W. Hong, K. S. Thygesen, S.-X. Liu, 'Controlling Electrical Conductance through a π-Conjugated Cruciform Molecule by Selective Anchoring to Gold Electrodes', *Angew. Chem. Int. Ed.* **2015**, *54*, 14304-14307.

[11] H. Li, P. Jiang, C. Yi, C. Li, S.-X. Liu, S. Tan, B. Zhao, J. Braun, W. Meier, T. Wandlowski, S. Decurtins, 'Benzodifuran-Based π-Conjugated Copolymers for Bulk Heterojunction Solar Cells', *Macromolecules* **2010**, *43*, 8058-8062.

[12] Y. Aeschi, H. Li, Z. Cao, S. Chen, A. Amacher, N. Bieri, B. Ozen, J. Hauser, S. Decurtins, S. Tan, S.-X. Liu, 'Directed Metalation Cascade To Access Highly Functionalized Thieno[2,3f|benzofuran and Exploration as Building Blocks for Organic Electronics', *Org. Lett.* **2013**, *15*, 5586-5589.

[13] C. Yi, C. Blum, M. Lehmann, S. Keller, S.-X. Liu, G. Frei, A. Neels, J. Hauser, S. Schurch, S. Decurtins, 'Versatile Strategy To Access Fully Functionalized Benzodifurans: Redox-Active Chromophores for the Construction of Extended π-Conjugated Materials', *J. Org. Chem.* **2010**, *75*, 3350-3357.

[14] A. Faurie, F. Gohier, P. Frere, 'Facile synthesis and optical properties of extended TPA-Benzodifuran derivatives connected by cyano-vinylene junctions', *Dyes Pigm.* **2018**, *154*, 38-43.

[15] Z. Kuang, G. He, H. Song, X. Wang, Z. Hu, H. Sun, Y. Wan, Q. Guo, A. Xia, 'Conformational Relaxation and Thermally Activated Delayed Fluorescence in Anthraquinone-Based Intramolecular Charge-Transfer Compound', *J. Phys. Chem. C* **2018**, *122*, 3727-3737.

[16] Q. Zhang, H. Kuwabara, W. J. Potscavage, S. Huang, Y. Hatae, T. Shibata, C. Adachi, 'Anthraquinone-Based Intramolecular Charge-Transfer Compounds: Computational Molecular Design, Thermally Activated Delayed Fluorescence, and Highly Efficient Red Electroluminescence', *J. Am. Chem. Soc.* **2014**, *136*, 18070-18081.

[17] J. Hankache, M. Niemi, H. Lemmetyinen, O. S. Wenger, 'Photoinduced Electron Transfer in Linear Triarylamine-Photosensitizer-Anthraquinone Triads with Ruthenium(II), Osmium(II), and Iridium(III)', *Inorg. Chem.* **2012**, *51*, 6333-6344.

[18] N. Dupont, Y.-F. Ran, H.-P. Jia, J. Grilj, J. Ding, S.-X. Liu, S. Decurtins, A. Hauser, 'Effect of the addition of a fused donor-acceptor ligand on a Ru(II) complex: synthesis, characterization, and photoinduced electron transfer reactions of [Ru(TTF-dppz)2(Aqphen)]2+', *Inorg. Chem.* **2011**, *50*, 3295-3303.

[19] A. Gouloumis, D. Gonzalez-Rodriguez, P. Vazquez, T. Torres, S. Liu, L. Echegoyen, J. Ramey, G. L. Hug, D. M. Guldi, 'Control Over Charge Separation in Phthalocyanine-Anthraquinone Conjugates as a Function of the Aggregation Status', *J. Am. Chem. Soc.* **2006**, *128*, 12674-12684.

[20] M. Kuss-Petermann, O. S. Wenger, 'Electron Transfer Rate Maxima at Large Donor-Acceptor Distances', *J. Am. Chem. Soc.* **2016**, *138*, 1349-1358.

[21] M. Frank, J. Ahrens, I. Bejenke, M. Krick, D. Schwarzer, G. H. Clever, 'Light-Induced Charge Separation in Densely Packed Donor-Acceptor Coordination Cages', *J. Am. Chem. Soc.* **2016**, *138*, 8279-8287.

[22] A. M. Shaikh, S. Chacko, R. M. Kamble, 'Synthesis, Optoelectronic and Theoretical Investigation of Anthraquinone Amine-Based Donor-Acceptor Derivatives', *ChemistrySelect* **2017**, *2*, 7620-7629.

[23] Y.-C. Hu, C.-J. Chen, H.-J. Yen, K.-Y. Lin, J.-M. Yeh, W.-C. Chen, G.-S. Liou, 'Novel triphenylamine-containing ambipolar polyimides with pendant anthraquinone moiety for polymeric memory device, electrochromic and gas separation applications', *J. Mater. Chem.* **2012**, *22*, 20394-20402.

[24] Y. Li, T. Tan, S. Wang, Y. Xiao, X. Li, 'Highly solvatochromic fluorescence of anthraquinone dyes based on triphenylamines', *Dyes Pigm.* **2017**, *144*, 262-270.

[25] A. M. Kini, D. O. Cowan, F. Gerson, R. Moeckel, 'New synthesis and properties of 11,11,12,12-tetracyano-9,10-anthraquinodimethane: an electron acceptor displaying a single-wave, two-electron reduction and a coproportionation pathway to the radical anion', *J. Am. Chem. Soc.* **1985**, *107*, 556-562.

[26] M. J. Bosiak, P. Trzaska, D. Kedziera, J. Adams, 'Synthesis and photoluminescence properties of star-shaped 2,3,6,7-tetrasubstituted benzo[1,2-b:4,5-b']difurans', *Dyes Pigm.* **2016**, *129*, 199-208.

[27] M. J. Bosiak, J. A. Jakubowska, K. B. Aleksandrzak, S. Kaminski, A. Kaczmarek-Kedziera, M. Ziegler-Borowska, D. Kedziera, J. Adams, 'Synthesis of a new class of highly fluorescent aryl-vinyl benzo[1,2-b:4,5-b']difuran derivatives', *Tetrahedron Lett* **2012**, *53*, 3923-3926.

[28] S. Keller, C. Yi, C. Li, S.-X. Liu, C. Blum, G. Frei, O. Sereda, A. Neels, T. Wandlowski, S. Decurtins, 'Synthesis, structures, redox and photophysical properties of benzodifuran-functionalized pyrene and anthracene fluorophores', *Org. Biomol. Chem.* **2011**, *9*, 6410-6416.

[29] R. Shukla, S. H. Wadumethrige, S. V. Lindeman, R. Rathore, 'Synthesis, Electronic Properties, and X-ray Structural Characterization of Tetrarylbenzo[1,2-b:4,5-b']difuran Cation Radicals', *Org. Lett.* **2008**, *10*, 3587-3590.

[30] J. E. Gautrot, P. Hodge, D. Cupertino, M. Helliwell, '2,6-Diaryl-9,10-anthraquinones as models for electron-accepting polymers', *New J. Chem.* **2007**, *31*, 1585-1593.

[31] A. Heckmann, C. Lambert, 'Organic Mixed-Valence Compounds: A Playground for Electrons and Holes', *Angew. Chem. Int. Ed.* **2012**, *51*, 326-392.

[32] H. Görner, 'Photoreduction of 9,10-Anthraquinone Derivatives: Transient Spectroscopy and Effects of Alcohols and Amines on Reactivity in Solution¶', *Photochem. Photobiol.* **2003**, *77*, 171-179.

[33] H. Li, R. Komatsu, J. Hankache, H. Sasabe, L. M. Lawson Daku, B. Özen, S. Chen, J. Hauser, A. Hauser, S. Decurtins, J. Kido, S.-X. Liu, 'Bis(Triphenylamine)Benzodifuran Chromophores: Synthesis, Electronic Properties and Application in Organic Light-Emitting Diodes', *Front. Chem.* **2021**, *9*, 721272

[34] M. Söderberg, B. Dereka, A. Marrocchi, B. Carlotti, E. Vauthey, 'Ground-State Structural Disorder and Excited-State Symmetry Breaking in a Quadrupolar Molecule', *J. Phys. Chem. Lett.* **2019**, *10*, 2944-2948.

[35] B. Dereka, E. Vauthey, 'Solute–Solvent Interactions and Excited-State Symmetry Breaking: Beyond the Dipole–Dipole and the Hydrogen-Bond Interactions', *J. Phys. Chem. Lett.* **2017**, *8*, 3927-3932.

[36] B. Dereka, A. Rosspeintner, R. Stężycki, C. Ruckebusch, D. T. Gryko, E. Vauthey, 'Excited-State Symmetry Breaking in a Quadrupolar Molecule Visualized in Time and Space', *J. Phys. Chem. Lett.* **2017**, *8*, 6029-6034.

[37] J. S. Beckwith, A. Rosspeintner, G. Licari, M. Lunzer, B. Holzer, J. Fröhlich, E. Vauthey, 'Specific Monitoring of Excited-State Symmetry Breaking by Femtosecond Broadband Fluorescence Upconversion Spectroscopy', *J. Phys. Chem. Lett.* **2017**, *8*, 5878-5883.

[38] E. Vauthey, 'Photoinduced Symmetry-Breaking Charge Separation', *ChemPhysChem* **2012**, *13*, 2001-2011.

[39] H. J. van Ramesdonk, B. H. Bakker, M. M. Groeneveld, J. W. Verhoeven, B. D. Allen, J. P. Rostron, A. Harriman, 'Ultrafast Intersystem Crossing in 9,10-Anthraquinones and Intramolecular Charge Separation in an Anthraquinone-Based Dyad', *J. Phys. Chem. A* **2006**, *110*, 13145-13150.

[40] N. Banerji, G. Duvanel, A. Perez-Velasco, S. Maity, N. Sakai, S. Matile, E. Vauthey, 'Excited-State Dynamics of Hybrid Multichromophoric Systems: Toward an Excitation Wavelength Control of the Charge Separation Pathways', *J. Phys. Chem. A* **2009**, *113*, 8202-8212.

[41] G. Duvanel, N. Banerji, E. Vauthey, 'Excited-State Dynamics of Donor−Acceptor Bridged Systems Containing a Boron−Dipyrromethene Chromophore: Interplay between Charge Separation and Reorientational Motion', *J. Phys. Chem. A* **2007**, *111*, 5361-5369.

[42] A. D. Becke, 'Density‐functional thermochemistry. III. The role of exact exchange', *J. Chem. Phys.* **1993**, *98*, 5648-5652.

[43] Becke3LYP. Method References and General Citation Guidelines in *Gaussian NEWS*, *Vol. 5, No.2*, Gaussian, Inc., Wallingford, CT, summer 1994.

[44] N. Godbout, D. R. Salahub, J. Andzelm, E. Wimmer, 'Optimization of Gaussian-type basis sets for local spin density functional calculations. Part I. Boron through neon, optimization technique and validation', *Can. J. Chem.* **1992**, *70*, 560-571.

[45] E. Aprà, E. J. Bylaska, W. A. de Jong, N. Govind, K. Kowalski, T. P. Straatsma, M. Valiev, H. J. J. van Dam, Y. Alexeev, J. Anchell, V. Anisimov, F. W. Aquino, R. Atta-Fynn, J. Autschbach, N. P. Bauman, J. C. Becca, D. E. Bernholdt, K. Bhaskaran-Nair, S. Bogatko, P. Borowski, J. Boschen, J. Brabec, A. Bruner, E. Cauët, Y. Chen, G. N. Chuev, C. J. Cramer, J. Daily, M. J. O. Deegan, T. H. Dunning, M. Dupuis, K. G. Dyall, G. I. Fann, S. A. Fischer, A. Fonari, H. Früchtl, L. Gagliardi, J. Garza, N. Gawande, S. Ghosh, K. Glaesemann, A. W. Götz, J. Hammond, V. Helms, E. D. Hermes, K. Hirao, S. Hirata, M. Jacquelin, L. Jensen, B. G. Johnson, H. Jónsson, R. A. Kendall, M. Klemm, R. Kobayashi, V. Konkov, S. Krishnamoorthy, M. Krishnan, Z. Lin, R. D. Lins, R. J. Littlefield, A. J. Logsdail, K. Lopata, W. Ma, A. V. Marenich, J. Martin del Campo, D. Mejia-Rodriguez, J. E. Moore, J. M. Mullin, T. Nakajima, D. R. Nascimento, J. A. Nichols, P. J. Nichols, J. Nieplocha, A. Otero-de-la-Roza, B. Palmer, A. Panyala, T. Pirojsirikul, B. Peng, R. Peverati, J. Pittner, L. Pollack, R. M. Richard, P. Sadayappan, G. C. Schatz, W. A. Shelton, D. W. Silverstein, D. M. A. Smith, T. A. Soares, D. Song, M. Swart, H. L. Taylor, G. S. Thomas, V. Tipparaju, D. G. Truhlar, K. Tsemekhman, T. Van Voorhis, Á. Vázquez-Mayagoitia, P. Verma, O. Villa, A. Vishnu, et al., 'NWChem: Past, present, and future', *J. Chem. Phys.* **2020**, *152*, 184102.

[46] M. E. Casida, Time-Dependent Density Functional Response Theory for Molecules in *Recent Advances in Density Functional Methods*, *Vol. 1* (Ed.: D. P. Chong), World Scientific, Singapore, 1995, pp. 155-192.

[47] S. Hirata, M. Head-Gordon, 'Time-dependent density functional theory within the Tamm–Dancoff approximation', *Chem. Phys. Lett.* **1999**, *314*, 291-299.

10.1002/hlca.202100099

Entry for the Table of Contents

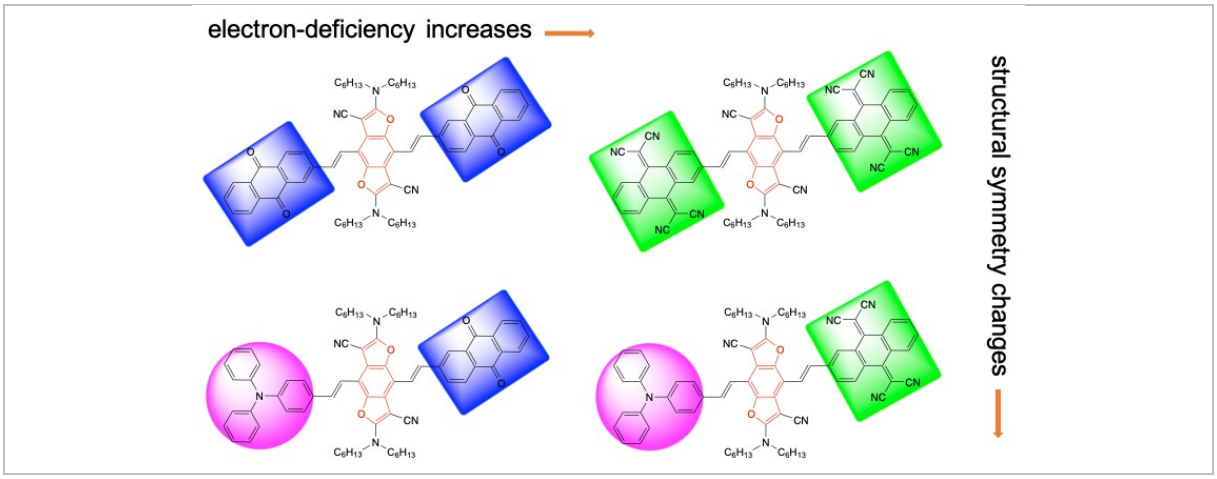

Twitter

The tweet text should not be more than 200 characters. Please describe your work with very short terms.